Conformal Fabrication of Colloidal Quantum Dot Solids for Optically Enhanced Photovoltaics

André J. Labelle,[†] Susanna M. Thon,[†,‡] Jin Young Kim,[†,§] Xinzheng Lan,[†,⊥] David Zhitomirsky,[†] Kyle W. Kemp,[†] and Edward H. Sargent*[,†]

[†]Department of Electrical and Computer Engineering, University of Toronto, 10 King's College Road, Toronto, Ontario M5S 3G4, Canada, [‡]Department of Electrical and Computer Engineering, Johns Hopkins University, 3400 North Charles Street, Baltimore, Maryland 21218, United States, [§]Fuel Cell Research Center, Korea Institute of Science and Technology (KIST), Seoul 136–791, South Korea, and [⊥]School of Materials Science and Engineering, Hefei University of Technology, 193 Tunxi Road, Hefei, Anhui Province 230009, People's Republic of China

ABSTRACT Colloidal quantum dots (CQD) are an attractive thin-film material for photovoltaic applications due to low material costs, ease of fabrication, and size-tunable band gap. Unfortunately, today they suffer from a compromise between light absorption and photocarrier extraction, a fact that currently prevents the complete harvest of incoming above-band-gap solar photons. We have investigated the use of structured substrates and/or electrodes to increase the effective light path through the active material and found that these designs require highly conformal application of the light-absorbing films to achieve the greatest enhancement. This conformality requirement derives from the need for maximal absorption enhancement combined with shortest-distance charge transport. Here we report on a means of processing highly conformal layer-by-layer deposited CQD absorber films onto microstructured, light-recycling electrodes. Specifically, we engineer surface hydrophilicity to achieve conformal deposition of upper layers atop underlying ones. We show that only with the application of conformal coating can we achieve optimal quantum efficiency and enhanced power conversion efficiency in structured-electrode CQD cells.

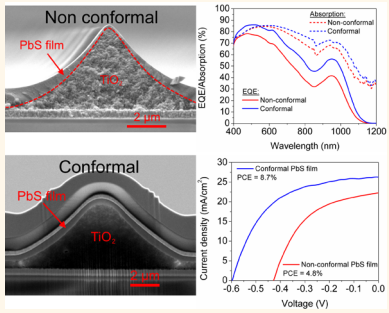

KEYWORDS: colloidal quantum dots · photovoltaics · solution-processed thin film · optically enhanced solar cells · conformal thin film · structured electrodes

Solution-processed colloidal quantum dot (CQD) photovoltaics are attractive for their low-cost fabrication and their reduced materials utilization compared to traditional photovoltaic technologies.[1−8] Because long diffusion lengths for photocarriers in CQD films have yet to be achieved, fully light-absorbing CQD films are too thick to extract all generated photocarriers with high efficiency, leading to an absorption−extraction compromise.[9,10] Device architectures have been developed that aim to overcome this compromise, including bulk heterojunctions,[11] depleted bulk heterojunctions,[12−16] and electrode structuring/geometry-based techniques. The latter provide for light recycling (multiple passes) through the active material *via* nanostructured substrates[17,18] and angled-device schemes that fold the path of light.[19] Bulk heterojunctions, which overcome limited charge transport by reducing the effective electrode−electrode distance, increase manyfold the junction area, which has a detrimental impact on open-circuit voltage since it heightens the bimolecular recombination rate at the increased-area interface.[20]

Absorption enhancement strategies can minimize the impact of increased effective interface area *via* careful selection and control over the texturing of the electrode; however, these strategies require conformal application of active materials atop the structured electrode. Only if made conformal will these propagate texture to the back-side mirror and also keep the contact-to-contact separation distance below the extraction thickness.

In the present work, we report a novel technique to deposit conformal solution-processed CQD thin films over structured substrates, an advance critical to leveraging light-recycling electrodes for enhanced power conversion efficiency (PCE) in thin-film photovoltaic cells.

* Address correspondence to ted.sargent@utoronto.ca.

Received for review February 27, 2015 and accepted April 16, 2015.

Published online April 16, 2015
10.1021/acsnano.5b01296

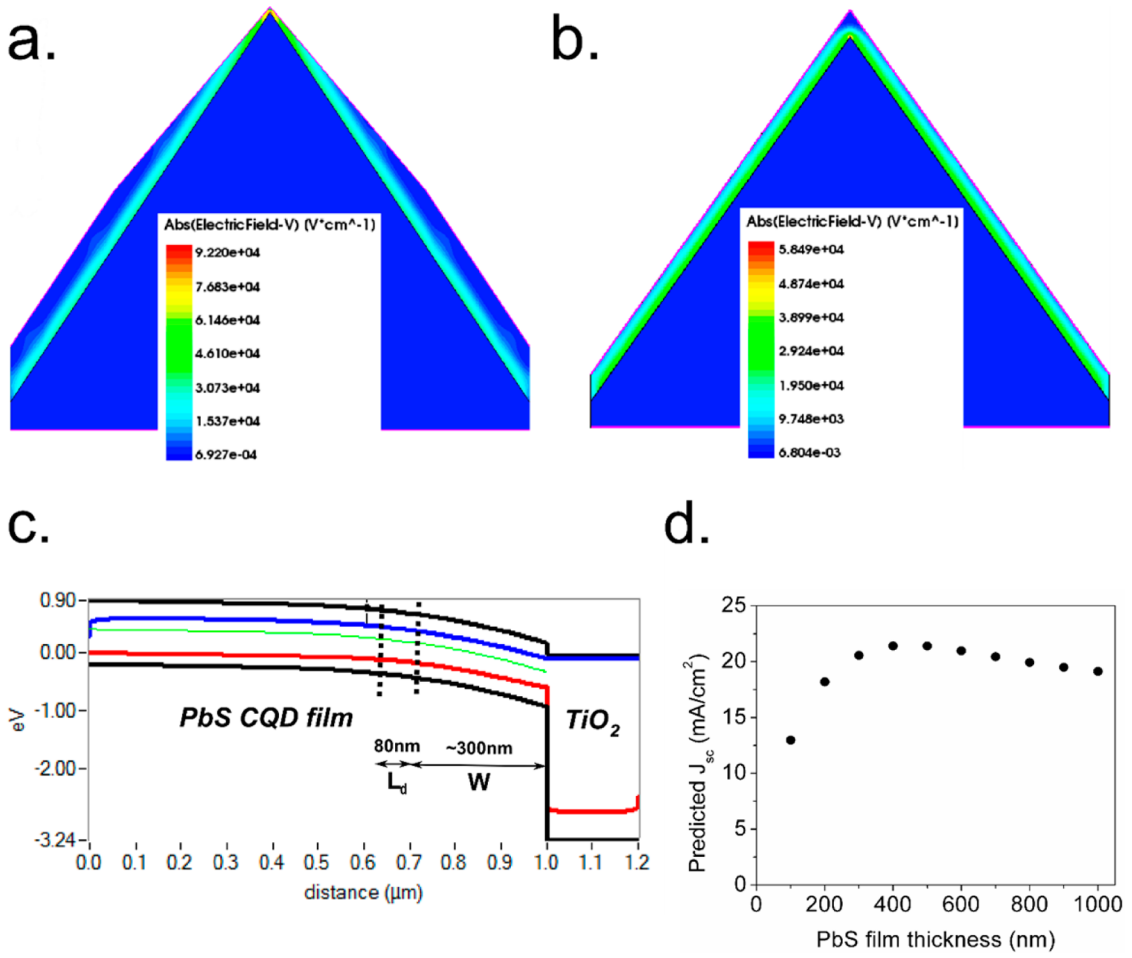

Figure 1. Simulated electric field distribution in a PbS CQD film (using the Sentaurus optoelectronic device modeling engine) in both a nonconformal (a) and conformal (b) context atop a pyramid-shaped electrode. (c) Band diagram of a depleted heterojunction CQD solar cell (PbS interfaced with TiO_2) to illustrate the band bending at short-circuit conditions and map out the depletion width and diffusion length in the PbS film. (d) Predicted short-circuit current density (J_{sc}) as a function of film thickness; we note that J_{sc} is optimized for a film thickness of 400 nm and then decreases for increased thickness despite the increased volume of absorptive material. This is considered the optimal thickness for charge extraction and absorption.

RESULTS AND DISCUSSION

To appreciate the enhancement potential of structured substrate strategies, we compared the impact on absorption enhancement of a number of different structures (Supporting Information S1). 3D finite-difference time-domain (FDTD) simulations were performed to determine the projected improvement for different periodic shapes with a standard periodicity of 2 μm $\times$ 2 μm. The simulations included the full layer structure of a depleted-heterojunction CQD solar cell,[21] including 300 nm thick 1.3 eV lead sulfide (PbS) CQD films on patterned/planar titania (TiO_2) electrodes. When we compared parabolic shapes, cones, and pyramids, we found a distinct improvement in absorption of longer-wavelength photons in all cases relative to the case of a planar sample of equal film thickness. In the most dramatic case, the structured electrodes led to improvements of 140%, 143%, and 165% at the most weakly absorbed wavelength (~840 nm) for parabola, cone, and pyramid structures, respectively. The best-case (internal quantum efficiency, IQE = 100%) short-circuit current density for the three classes of structures relative to the planar control resulted in improvements of 29%, 33%, and 40% for the parabola, cone, and pyramid features, respectively. We attribute the high performance of the pyramid design to its high areal packing density of the structured elements: the pyramids lack planar plateaus/mesas present in the case of structures based on circular-base periodically arrayed repeat units. A more detailed analysis of the absorption-enhancement potential of microstructured pyramid electrodes is reported elsewhere.[22]

We sought to explore in simulation the importance of ensuring that the absorbing film is *conformal* over the structured electrode. We used Sentaurus (3D self-consistent optoelectronic device modeling software) to compare conformal *vs* nonconformal films on a pyramid-shaped electrode for 1.3 eV CQD layers (Figure 1a,b). The built-in electric field in the light-absorbing CQD film is, in the nonconformal case, much

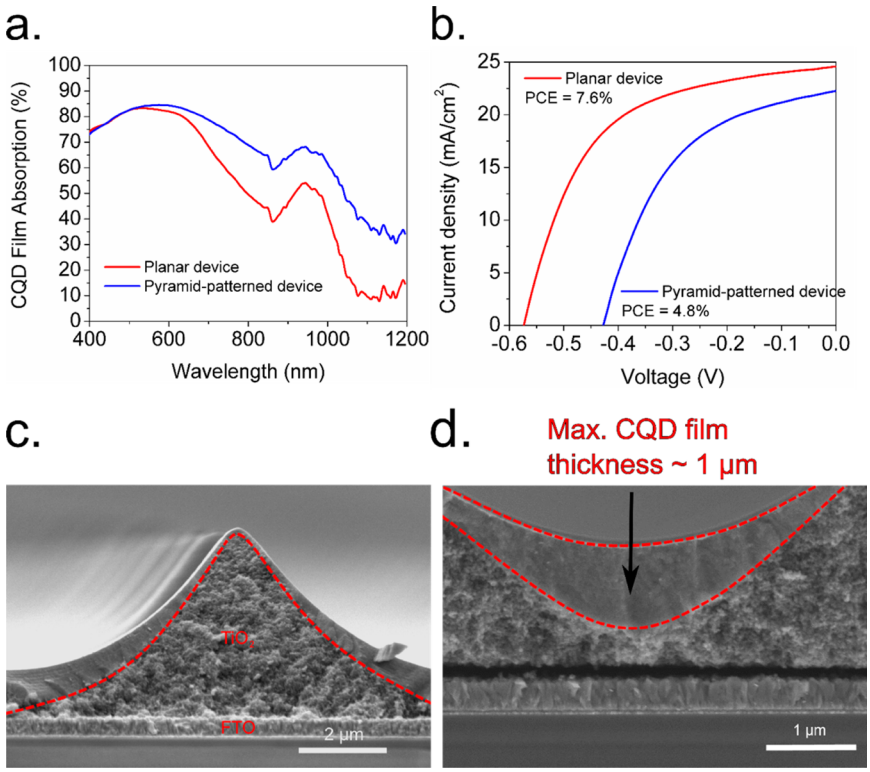

Figure 2. Nonconformal CQD films. (a) Full-pass CQD film absorption comparing a pyramid-patterned sample to its planar control. Note the drastic improvement in absorption at wavelengths >700 nm for the pyramid-patterned sample. (b) Current–voltage measurements under simulated AM1.5 illumination of a PbS device prepared using spin-coated film fabrication techniques. Note that device performance is significantly lower than the planar control despite absorption enhancement in the pyramid-patterned case. (c) Scanning electron microscopy (SEM) image of a pyramid-patterned substrate overcoated with a PbS CQD film deposited using conventional techniques. Note the inconsistent film thickness with very thin regions at the apex and increasingly thick regions in the valleys. (d) Magnified SEM image of the pyramid valley with nonconformal CQD film thickness is measured to exceed 1 μm in this case.

less favorable to drift-based charge extraction. It includes regions of reduced *E*-field strength where the film thickness exceeds the optimal collection distance (Figure 1a). In the conformal case, a uniformly distributed electric field serves to sweep photogenerated charges from the device in all locations within the light-absorbing film (Figure 1b).

Using additional modeling, we found that the film thickness beyond which charge extraction efficiency degrades is roughly given by the sum of the depletion width and the diffusion length for photogenerated charges in the absorbing material. This optimal length for charge extraction is illustrated in the spatial band diagram of a 1.3 eV CQD film interfaced with TiO_2 (Figure 1c). A doping density of $\sim 10^{16}$ cm^{-3} is assumed in the TiO_2 material,[2] in which case the depletion width extends into the CQD film over about ~300 nm. The diffusion length has been determined to be ~80 nm for hybrid-passivated CQD solids,[10] indicating an extraction length of ~380 nm (Figure 1c). More quantitatively, we plot the short-circuit current density (J_{sc}) as a function of film thickness (Figure 1d). The predicted J_{sc} is indeed optimized for a PbS film thickness of 400 nm ($W \approx$ 300 nm and L_d = 80 nm) and then decreases for thicker films despite the increased volume of absorbing material.

We applied a stamp-transfer method to prepare pyramid-patterned TiO_2 electrodes.[22] Our purpose was to prepare CQD photovoltaic devices that would leverage increased optical absorption and proportionate improvements in J_{sc}, leading to improved overall PCE.

In early studies, when preparing the absorbing CQD films, we used previously reported film deposition techniques.[1] Spin-coating of oleic acid-capped 1.3 eV CQDs was followed by a solid-state ligand exchange using 3-mercaptopropionic acid (3-MPA) in a hybrid passivation approach.[1] Full-pass absorption measurements reveal a significant improvement for the pyramid-patterned CQD device compared to the planar control for $\lambda >$ 700 nm, consistent with optical modeling predictions. The most dramatic enhancement was observed at ~850 nm wavelength with an approximately 45% increase in absorption (Figure 2a).

However, in spite of these substantial absorption enhancements, the pyramid-patterned device exhibited current–voltage characteristics under simulated AM1.5 illumination that revealed a notable loss in V_{oc} (26%), fill factor (FF) (12%), J_{sc} (9%), and consequently PCE (37%) compared to planar controls (Figure 2b). Scanning electron microscopy (SEM) revealed nonconformal coverage of the CQD film over the full extent of

the pyramid features (Figure 2c). Specifically, the CQD absorber was excessively (>1 μm) thick in the valleys between pyramids and formed a sub-100 nm thick film at the apexes. At higher magnification, SEM further illustrates this inconsistency in film thickness, with a roughly 1 μm collection distance at the thickest point in the film (Figure 2d). The thick regions of the film are expected to reduce charge extraction efficiency and increase series resistance; furthermore, in the regions beyond the depletion width of the film (>400 nm), photogenerated carriers mainly recombine, compromising the open-circuit voltage of the cell. The thin regions at the pyramid peaks represent lost optical absorption opportunities and, worse still, potential shunting paths.

We sought therefore to develop a procedure to provide conformal deposition of CQD films atop textured substrates. We took the view that it would be advantageous to reduce the extent to which the (hydrophobic) solvent used to introduce the CQDs would wet the patterned substrate surface. A low-concentration primer solution of 3-MPA in methanol was applied to the electrode surface prior to solid-state fabrication of the CQD film and was reapplied between every successive layer. The primer treatment is expected to create a monolayer of 3-MPA on the surface and thereby modify the surface affinity, leading to conformal coating of subsequent PbS CQD layers. We used 3-MPA for compatibility with the CQD film and for its hydrophilic nature.

To understand the impact of the ligand-primer treatment on conformal film formation, we performed contact angle measurements on a planar TiO_2 substrate prepared using the same material and treatments as used for pyramid-patterned electrodes. Prior to treatment, the contact angle for a 4 μL drop of H_2O was measured to be 39° (Figure 3a). The contact angle for an identical volume of H_2O was measured to be 29° (Figure 3b) following ligand-primer treatment of the substrate. The reduction in contact angle indicates an increased affinity between the surface and the hydrophilic liquid following ligand-primer treatment. Since the quantum dots (QDs) are dispersed in a hydrophobic solvent, the opposite effect will occur on the QD solution; that is, the surface will repel the solution. Wetting properties for patterned surfaces are qualitatively distinct compared to planar counterparts (capillary forces cause preferential in-filling of porous regions of the structures[23]), leading to a liquid meniscus effect between adjacent features. With the ligand-primer treatment applied in this study, the surface becomes more repellant to the QD solvent and modifies the wetting behavior, allowing air to create a separation between the solvent and the surface while the substrate is retracted from the QD solution during film fabrication. This prevents relaxation of the QD-containing solvent in the pyramid valleys, ultimately preventing the nonuniform film formation that otherwise occurs as the solvent dries. This method is, in principle, adaptable and could be used to conformally coat structured features on a variety of length scales for applications in diverse optoelectronic devices.

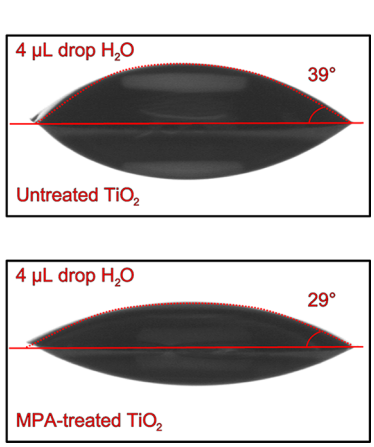

Figure 3. Contact angle measurements of wetting-engineered surface. (a) Contact angle measurement of an untreated TiO_2 electrode (using 4 μL of deionized H_2O). The contact angle was computed as an average of 39°. (b) Contact angle measurement of a ligand-primer-treated TiO_2 electrode (using 4 μL of deionized H_2O, again). In this case the contact angle is reduced to 29°, indicative that this treatment increases the surface affinity for hydrophilic liquids.

By applying this ligand-primer technique coupled with dip-coating deposition, we were able to prepare highly conformal films. SEM images of focused-ion-beam (FIB) milled cross-sections reveal the highly conformal CQD films deposited using this technique (Figure 4a). Higher-magnification SEM images reveal the film to be approximately 400 nm in thickness over a large range of the pyramid features, close to the optimal film thickness for efficient charge extraction (Figure 4b). For added confirmation we include a top-view SEM of an area ~50 × 50 μm^2 of the pyramid-patterned surface showing CQD films to be conformal over an array of 25 pyramid features (Figure 4c).

Investigating quantitatively, we compared the internal quantum efficiency, a measure of charge extraction efficiency, for CQD pyramid-patterned devices prepared using conventional spin-coating methods, standard dip-coating, and dip-coating combined with the ligand-primer treatment (Figure 4d). Compared to the nonconformal spin-coated case, we observed a global improvement of IQE over all wavelengths when we employed similarly nonconformal passive-drying deposition techniques such as dip-coating. With the addition of surface functionalization *via* MPA primer treatment we observe a similar, more quantitatively significant global improvement for all wavelengths compared to the nonconformal cases. We further note improved charge extraction efficiency for photons of λ > 850 nm compared to the dip-coated case without the ligand-primer treatment. The IQE is most improved at the exciton peak (~960 nm) when we use the primer

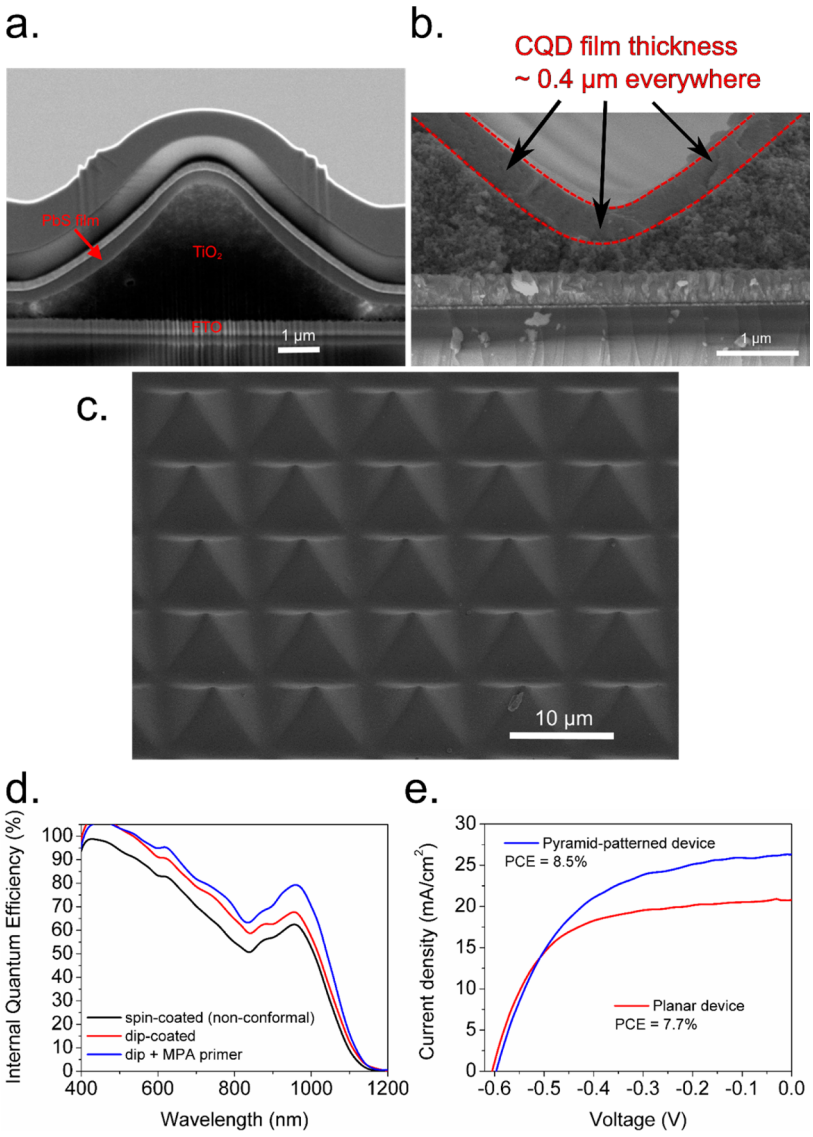

Figure 4. Conformal CQD films. (a) SEM image of a focus-ion-beam-milled cross-section illustrating the resulting device when applying dip-coating + ligand-primer treatment to the pyramid-patterned TiO_2 electrode. The film thickness is consistent over the surface of the pyramid with this treatment. (b) Magnified SEM of the pyramid valley with conformal CQD film thickness is measured to be ~400 nm over the full range of the image. (c) Large-area SEM image illustrating the uniform film coverage across the device. (d) Internal quantum efficiency of pyramid-patterned devices prepared with three distinct fabrication methods. Dip-coated samples are distinctly superior in quantum efficiency as compared to spin-coated samples; we further note improved quantum efficiency when employing ligand primer to the dip-coated film in the most weakly extracted wavelengths for PbS CQD films (850−1050 nm), with approximately 17% improvement in quantum efficiency at the exciton peak. Note that IQE exceeds 100% in some cases due to propagating uncertainties from absorption and external quantum efficiency measurements. (e) Current−voltage measurement under simulated AM1.5 illumination comparing a pyramid-patterned device prepared with ligand-primer treatment to a planar control. The J_{sc} improves by an amount proportional to the absorption enhancement of the structure, with negligible compromise in V_{oc} and FF, ultimately leading to improved PCE.

technique, providing enhancements of 26% and 17% relative to the reference spin-coated and dip-coated cases, respectively. We attribute this dramatic improvement in device IQE to the improved conformality of the CQD film, which allows for efficient extraction of photogenerated carriers from a larger total volume of the light-absorbing film.

With the application of ligand-primer treatment we were able to optimize charge extraction and achieve improved device performance for pyramid-patterned CQD samples. Current−voltage measurements under simulated AM1.5 illumination reveal a representative PCE of 8.5% using a pyramid-patterned TiO_2 electrode compared to a planar control PCE of 7.7% (Figure 4e). With conformal CQD films we find minimal compromise in V_{oc} and FF (no change in V_{oc} and 11% reduction in FF). The major improvement is in J_{sc} (increased by 27%) for a global improvement in power conversion efficiency (10% improvement in this case).

To highlight the reproducibility of our technique, we include statistics comparing conformally coated pyramid-patterned samples with planar controls

(Supporting Information S2). From a sample set of 36 optimal pyramid-patterned devices (*i.e.*, individual 0.049 cm^2 devices), we measured an average PCE of 7.9 $\pm$ 0.4% with an average J_{sc} of 25.2 $\pm$ 1.6 mA/cm^2. For a set of 27 planar devices prepared using similar dip-coating conditions, we find an average PCE of 6.2 $\pm$ 1.1% with an average J_{sc} of 19.8 $\pm$ 2.3 mA/cm^2. On average, the conformally coated structured samples yield an improvement of 27% in both J_{sc} and PCE above planar controls, proving the repeatability and significance of conformal coating when applied to structured CQD solar cells.

CONCLUSION

The deposition of CQD films conformally onto structured substrates has applications within, and potentially beyond, photovoltaics. Its benefits could potentially be realized in the formation of photodetector arrays on curved and structured substrates; in the fabrication of wide-viewing-angle displays; and in coating active layers on 3D-structured cavities to form lasers such as in whispering-gallery-mode (WGM) devices. In the photovoltaics context, the technique yielded a notable performance improvement when CQD films were deposited on pyramid-patterned electrodes. Conformal films atop the structured substrate produced proportional improvements in J_{sc} and power conversion efficiency relative to corresponding planar controls, validating the method in enabling photonically enhanced CQD photovoltaics.

METHODS

Device Simulations. One-dimensional device simulations were performed using SCAPS 3.0.01 software. The device model was adapted from previously published work.[24] Finite-difference time-domain simulations were carried out using Lumerical FDTD Solutions software (http://www.Lumerical.com) version 8.7.4. All simulations were carried out in 3D for pyramids, parabola, cones, or planar structures with periodic boundary conditions in the *x* and *y* directions and a unit size of 2000 $\times$ 2000 nm^2. A broadband (λ = 400−1200 nm) planewave source polarized along the *y*-axis was incident from within the glass region. The absorption was isolated for the individual layers, only the absorption of the CQD layer is presented in Figure 1a, and projected short-circuit current density was calculated in Figure 1b assuming an IQE of 100% and integrating over the AM1.5 solar spectrum.

Electrode Preparation. Pyramid-patterned TiO_2 substrates were prepared with polydimethylsiloxane (PDMS) stamps patterned with inverted pyramidal features (with a periodicity of 10 μm) that were molded from a silicon master. These were all prepared applying previously published techniques.[22]

Device Fabrication. All spin-coated samples (pyramid-patterned and planar controls) were prepared using a layer-by-layer spin-cast deposition method. PbS quantum dots (synthesized and exchanged following previously published protocols[1]) were deposited at a concentration of 50 mg/mL in octane through a 0.2 μm filter, followed by solid-state exchange using 3-mercaptopropionic acid at a concentration of 1% v/v in methanol. Finally, the film was rinsed twice with pure methanol. All samples were spin-cast at 2500 rpm for a total of 10 cycles. All dip-coated devices (pyramid-patterned and planar controls) were prepared using sequential dip-coating. Samples were manipulated using a medium-sized KSV NIMA multivessel dip-coater. The samples with MPA primer treatment were first dipped into 30 mL beakers containing 15 mL of 0.05% v/v 3-MPA in methanol for 5 s, then left to dry for 360 s (surface primer treatment). Samples were then dipped into an adjacent 30 mL beaker containing 15 mL of 7.5 mg/mL PbS quantum dots (same as used for spin-casting) in hexane for 30 s and left to dry for 240 s. Samples were then dipped into a 50 mL beaker containing 25 mL of 0.2% v/v MPA in methanol solution (solid-state exchange) for 3 s followed by 60 s drying. Finally the samples were rinsed in a 50 mL beaker containing 25 mL of pure methanol for 5 s and dried for 120 s. This process was repeated for 10−18 cycles for optimal results (number of cycles being dependent on room humidity). Note that samples without MPA primer treatment were fabricated using the same sequence, minus the first step with 0.05% MPA. All top contacts were deposited *via* thermal (molybdenum trioxide and silver) and e-beam (gold) evaporation in an Angstrom Engineering deposition system inside an Innovative Technology glovebox. Total thickness of each material was 30−40 nm MoO_3 (deposited at a rate of 1 Å/s), 55 nm Au (deposited at a rate of 1.5 Å/s), and 200 nm Ag (deposited at a rate of 3 Å/s).

Absorption Measurements. The procedures used for these measurements are similar to those published by Adachi *et al.*[17] All absorption measurements were done using a PerkinElmer Lambda 950 UV−vis−NIR spectrophotometer equipped with an integrating sphere. Samples were placed at the center of the integrating sphere tilted at an angle of 20° relative to the incident beam. The total transmission (*T*) and reflectance (*R*) were collected by the integrating sphere detector with all ports closed except the one for the incident beam. Absorption was calculated as 100% $-$ *T* $-$ *R*. The 100% transmission baseline measurement was an empty sphere. Full-pass absorption was calculated using single-pass absorption data for all active films; details are provided in Supporting Information S3.

AM1.5 Photovoltaic Device Characterization. The procedures used for these measurements are similar to those published by Adachi *et al.*[17] All photovoltaic and EQE measurements were carried out under N_2 flow. Current density−voltage curves were measured using a Keithley 2400 source meter with illumination from a Sciencetech solar simulator with an irradiance of 100 mW/cm^2. The active area of the solar cell was illuminated through a circular aperture with an area of 0.049 cm^2. The power was measured using a Melles-Griot broadband power meter. The spectral mismatch between measured and actual solar spectrum was measured using a calibrated reference solar cell from Newport. A total spectral mismatch of ~4% was taken into account by applying a multiplicative factor of 0.96 to the measured current density values. The uncertainty of AM1.5 measurements was estimated to be $\pm$7%.

External Quantum Efficiency Measurements. The procedures used for these measurements are identical to those published by Adachi *et al.*[17] External quantum efficiency spectra were measured under monochromatic light (400 W xenon lamp source passing through a monochromator with order-sorting filters) that was chopped at 220 Hz. A constant 1-sun intensity white-light source simultaneously illuminated the device during measurements. The monochromatic light power was measured using Newport 818-UV and Newport 818-IR power meters. The current response was measured using a Stanford Research Systems lock-in amplifier at short-circuit conditions. The uncertainty of the EQE measurements, calculated from taking the root-mean-square of the error from all equipment, was $\pm$3%.

Internal Quantum Efficiency Calculations. Details are provided in Supporting Information S4.

Contact Angle Measurements. Contact angle measurements were carried out using a Kruss DSA100 drop shape analysis system using the static Sessile drop method. Planar substrates were prepared with a TiO_2 solution (1:2 Dyesol DS90 TiO_2 nanoparticles/ethanol) spin-coated onto an FTO-coated glass substrate at 1500 rpm for 10 s. Planar substrates were then

heat-treated and $TiCl_4$-treated according to the same protocol used for pyramid-patterned substrates. A 4 μL drop of deionized water was deposited on the substrate while in the DSA100 system. Corresponding software captured magnified images of the droplet and calculated the contact angle from a modeled circular shape of the image.

Conflict of Interest: The authors declare no competing financial interest.

Acknowledgment. This publication is based in part on work supported by Award KUS-11-009-21, made by King Abdullah University of Science and Technology (KAUST), by the Ontario Research Fund Research Excellence Program, and by the Natural Sciences and Engineering Research Council (NSERC) of Canada. The authors thank Larissa Levina for assistance in the CQD synthesis, Oleksandr Voznyy for assistance with SCAPS modeling software, and Elenita Palmiano, Remi Wolowiec, Ghada Koleilat, Silvia Masala, Haopeng Dong, and Damir Kopilovic for their technical help over the course of this study. A.J.L., S.M.T., and E. H.S. designed the study. A.J.L. prepared and characterized (AM1.5, absorption, EQE) all samples and analyzed all data, with assistance from K.W.K. A.J.L. and J.Y.K. performed contact angle measurements. A.J.L. performed FDTD and SCAPS simulations, while D.Z. performed Sentaurus optoelectronic device simulations. A.J.L. and X.L. developed and optimized procedures for dip-coating CQD devices. A.J.L. wrote the manuscript with feedback from S.M.T. and E.H.S.

Supporting Information Available: Four supplementary figures included to highlight the theoretical optical advantages of structured substrates, to provide PCE statistics to demonstrate reproducibility of conformal film technique, and to describe the methods used to calculate absorption of thin films over structured substrates as well as calculations for internal quantum efficiency. This material is available free of charge *via* the Internet at http://pubs.acs.org.

REFERENCES AND NOTES

1. Ip, A. H.; Thon, S. M.; Hoogland, S.; Voznyy, O.; Zhitomirsky, D.; Debnath, R.; Levina, L.; Rollny, L. R.; Carey, G. H.; Fischer, A.; *et al*. Hybrid Passivated Colloidal Quantum Dot Solids. *Nat. Nanotechnol.* **2012**, *7*, 577–582.
2. Wang, X.; Koleilat, G. I.; Tang, J.; Liu, H.; Kramer, I. J.; Debnath, R.; Brzozowski, L.; Barkhouse, D. A. R.; Levina, L.; Hoogland, S.; *et al*. Tandem Colloidal Quantum Dot Solar Cells Employing a Graded Recombination Layer. *Nat. Photonics* **2011**, *5*, 480–484.
3. Choi, J. J.; Wenger, W. N.; Hoffman, R. S.; Lim, Y.-F.; Luria, J.; Jasieniak, J.; Marohn, J. A.; Hanrath, T. Solution-Processed Nanocrystal Quantum Dot Tandem Solar Cells. *Adv. Mater.* **2011**, *23*, 3144–3148.
4. Chuang, C.-H. M.; Brown, P. R.; Bulović, V.; Bawendi, M. G. Improved Performance and Stability in Quantum Dot Solar Cells through Band Alignment Engineering. *Nat. Mater.* **2014**, *13*, 796–801.
5. Munechika, K.; Chen, Y.; Tillack, A. F.; Kulkarni, A. P.; Jen-La Plante, I.; Munro, A. M.; Ginger, D. S. Quantum Dot/Plasmonic Nanoparticle Metachromophores with Quantum Yields That Vary with Excitation Wavelength. *Nano Lett.* **2011**, *11*, 2725–2730.
6. Tang, J.; Liu, H.; Zhitomirsky, D.; Hoogland, S.; Wang, X.; Furukawa, M.; Levina, L.; Sargent, E. H. Quantum Junction Solar Cells. *Nano Lett.* **2012**, *12*, 4889–4894.
7. Tang, J.; Kemp, K. W.; Hoogland, S.; Jeong, K. S.; Liu, H.; Levina, L.; Furukawa, M.; Wang, X.; Debnath, R.; Cha, D.; *et al*. Colloidal-Quantum-Dot Photovoltaics Using Atomic-Ligand Passivation. *Nat. Mater.* **2011**, *10*, 765–771.
8. Fischer, A.; Rollny, L.; Pan, J.; Carey, G. H.; Thon, S. M.; Hoogland, S.; Voznyy, O.; Zhitomirsky, D.; Kim, J. Y.; Bakr, O. M.; *et al*. Directly Deposited Quantum Dot Solids Using a Colloidally Stable Nanoparticle Ink. *Adv. Mater.* **2013**, *25*, 5742–5749.
9. Clifford, J. P.; Konstantatos, G.; Johnston, K. W.; Hoogland, S.; Levina, L.; Sargent, E. H. Fast, Sensitive and Spectrally Tuneable Colloidal-Quantum-Dot Photodetectors. *Nat. Nanotechnol.* **2009**, *4*, 40–44.
10. Zhitomirsky, D.; Voznyy, O.; Hoogland, S.; Sargent, E. H. Measuring Charge Carrier Diffusion in Coupled Colloidal Quantum Dot Solids. *ACS Nano* **2013**, *7*, 5282–5290.
11. Rath, A. K.; Bernechea, M.; Martinez, L.; de Arquer, F. P. G.; Osmond, J.; Konstantatos, G. Solution-Processed Inorganic Bulk Nano-Heterojunctions and Their Application to Solar Cells. *Nat. Photonics* **2012**, *6*, 529–534.
12. Kramer, I. J.; Zhitomirsky, D.; Bass, J. D.; Rice, P. M.; Topuria, T.; Krupp, L.; Thon, S. M.; Ip, A. H.; Debnath, R.; Kim, H.-C.; *et al*. Ordered Nanopillar Structured Electrodes for Depleted Bulk Heterojunction Colloidal Quantum Dot Solar Cells. *Adv. Mater.* **2012**, *24*, 2315–2319.
13. Lan, X.; Bai, J.; Masala, S.; Thon, S. M.; Ren, Y.; Kramer, I. J.; Hoogland, S.; Simchi, A.; Koleilat, G. I.; Paz-Soldan, D.; *et al*. Self-Assembled, Nanowire Network Electrodes for Depleted Bulk Heterojunction Solar Cells. *Adv. Mater.* **2013**, *25*, 1769–1773.
14. Barkhouse, D. A. R.; Debnath, R.; Kramer, I. J.; Zhitomirsky, D.; Pattantyus-Abraham, A. G.; Levina, L.; Etgar, L.; Grätzel, M.; Sargent, E. H. Depleted Bulk Heterojunction Colloidal Quantum Dot Photovoltaics. *Adv. Mater.* **2011**, *23*, 3134–3138.
15. Wang, H.; Kubo, T.; Nakazaki, J.; Kinoshita, T.; Segawa, H. PbS-Quantum-Dot-Based Heterojunction Solar Cells Utilizing ZnO Nanowires for High External Quantum Efficiency in the Near-Infrared Region. *J. Phys. Chem. Lett.* **2013**, *4*, 2455–2460.
16. Jean, J.; Chang, S.; Brown, P. R.; Cheng, J. J.; Rekemeyer, P. H.; Bawendi, M. G.; Gradečak, S.; Bulović, V. ZnO Nanowire Arrays for Enhanced Photocurrent in PbS Quantum Dot Solar Cells. *Adv. Mater.* **2013**, *25*, 2790–2796.
17. Adachi, M. M.; Labelle, A. J.; Thon, S. M.; Lan, X.; Hoogland, S.; Sargent, E. H. Broadband Solar Absorption Enhancement *via* Periodic Nanostructuring of Electrodes. *Sci. Rep.* **2013**, *3*, 2928.
18. Mahpeykar, S. M.; Xiong, Q.; Wang, X. Resonance-Induced Absorption Enhancement in Colloidal Quantum Dot Solar Cells Using Nanostructured Electrodes. *Opt. Express* **2014**, *22*, A1576–A1588.
19. Koleilat, G. I.; Kramer, I. J.; Wong, C. T. O.; Thon, S. M.; Labelle, A. J.; Hoogland, S.; Sargent, E. H. Folded-Light-Path Colloidal Quantum Dot Solar Cells. *Sci. Rep.* **2013**, *3*, 2166.
20. Kemp, K. W.; Labelle, A. J.; Thon, S. M.; Ip, A. H.; Kramer, I. J.; Hoogland, S.; Sargent, E. H. Interface Recombination in Depleted Heterojunction Photovoltaics Based on Colloidal Quantum Dots. *Adv. Energy Mater.* **2013**, *3*, 917–922.
21. Pattantyus-Abraham, A. G.; Kramer, I. J.; Barkhouse, A. R.; Wang, X.; Konstantatos, G.; Debnath, R.; Levina, L.; Raabe, I.; Nazeeruddin, M. K.; Grätzel, M.; *et al*. Depleted-Heterojunction Colloidal Quantum Dot Solar Cells. *ACS Nano* **2010**, *4*, 3374–3380.
22. Labelle, A. J.; Thon, S. M.; Masala, S.; Adachi, M. M.; Dong, H.; Farahani, M.; Ip, A. H.; Fratalocchi, A.; Sargent, E. H. Colloidal Quantum Dot Solar Cells Exploiting Hierarchical Structuring. *Nano Lett.* **2014**, *15*, 1101–1108.
23. Bico, J.; Thiele, U.; Quéré, D. Wetting of Textured Surfaces. *Colloids Surf. Physicochem. Eng. Asp.* **2002**, *206*, 41–46.
24. Zhitomirsky, D.; Voznyy, O.; Levina, L.; Hoogland, S.; Kemp, K. W.; Ip, A. H.; Thon, S. M.; Sargent, E. H. Engineering Colloidal Quantum Dot Solids within and beyond the Mobility-Invariant Regime. *Nat. Commun.* **2014**, *5*, 3803.